J Mater Sci (2011) 46:2437–2444
DOI 10.1007/s10853-010-5090-3

Investigation of the mechanism of self-propagating high-temperature synthesis of TiNi

Han-Qing Che · Yan Ma · Qun-Cheng Fan

Received: 19 July 2010 / Accepted: 16 November 2010 / Published online: 2 December 2010

Abstract An improved combustion front quenching method was used to investigate the mechanism of self-propagating high-temperature synthesis (SHS) of TiNi from Ti and Ni powders. The microstructural evolution in the quenched sample was observed with scanning electron microscope (SEM) and analyzed with energy dispersive X-ray spectrometry. Also, the combustion temperature of the reaction was measured, and the phase constituent of the synthesized product was inspected by X-ray diffraction. Based on those experimental results, a dissolution–precipitation–diffusion mechanism was proposed and compared with those mechanisms concluded by other authors, thus the mechanism for the SHS of TiNi was systematically discussed. In addition, the influence and necessity of preheating before the ignition was discussed.

Introduction

TiNi shape memory alloy (SMA) has been recently acknowledged as a very important functional material, especially as biomaterial because of its excellent mechanical property, good corrosion resistance, high biocompatibility, special pseudo elasticity as well as shape and volume memory effect [1–4]. Also, porous TiNi possesses high recoverable strain that closely matches the characteristics of natural bone and it allows the growth of bone tissue into the implant [4–6].

TiNi can be fabricated by means of combustion synthesis (CS) which is a well-known technique used to prepare a variety of materials due to its unique advantages [7]. Recently, preparation of TiNi intermetallic compounds by combustion synthesis had been performed in both thermal explosion (TE) mode [8–14] and in self-propagating high-temperature synthesis (SHS) mode [15–21]. On one hand, with the TE mode, Biswas [11] investigated the reaction mechanism of TiNi by intercepting the combustion at different stages during the reaction, and pointed out that the combustion mechanism could be described as the solid-state diffusion followed by the contact melting and the liquid-assisted reactive diffusion. On the other hand, by means of SHS, Li et al. [15] indicated that the diffusion and the capillary action were the main reaction mechanism in their study of SHS of porous TiNi. While Dey [16] examined the mechanism of synthesis in the case of unpreheated specimens and claimed that the Ni particles melted first and engulfed the Ti particles, triggering the combustion; and the phase evolution started from the Ni-rich phases like Ni_4Ti and moved progressively toward the Ti-rich phases; ultimately, the reaction of Ni with Ti_2Ni_3 and Ti resulted in the formation of TiNi. However, Dey's work was not based on the traditional SHS method and conflicted with others' since the adiabatic temperature (T_{ad}) [15] of the combustion reaction in the case without preheating is lower than the melting temperature of Ni. Furthermore, it was reported previously that preheating the sample before the ignition is necessary to achieve self-sustained combustion during synthesis of TiNi due to the relatively low exothermic characteristic of the reaction itself, and the SHS cannot propagate when the preheating temperature is below 150 °C [15]. In sum, although there were a lot of researches on the combustion synthesis of TiNi, the microstructural evolution during the SHS of TiNi is still not very clear or evident, and further investigation is indeed needed.

H.-Q. Che · Y. Ma · Q.-C. Fan (✉)
State Key Laboratory for Mechanical Behavior of Materials, Xi'an Jiaotong University, Xi'an 710049, China
e-mail: qcfan@mail.xjtu.edu.cn

To investigate the mechanism of the self-propagating reaction, Rogachev et al. [22] invented the so-called combustion front quenching method (CFQM) to obtain a specimen with reacted area, reacting area, and unreacted area in it. Subsequent SEM observation could show the microstructural evolution during the synthesis so that a mechanism of the synthesis could be proposed. Fan et al. improved the CFQM (details of the improvement was reported previously [23]), and studied mechanisms of SHS of $TiAl_3$ [23], TiC–Fe composite [24, 25], β-NiAl(Cu)/α(Cu, Ni) composite [26], TiC–Al cermet [27], TiC–Ti cermet [28], TiC–Ni cermet [29], Ni_2Al_3 compound [30], etc.

In this study, the improved CFQM was used for investigating the microstructural evolution during SHS of TiNi compound from Ti and Ni powder mixture. The microstructural evolution in the quenched specimen was observed with SEM and analyzed with EDX. In addition, the temperature–time profile of the combustion reaction was measured and the phase constituent of the combustion-synthesized product was inspected by XRD. Based on these experimental results, the mechanism of the combustion synthesis was discussed.

Experimental procedures

Titanium powder (125–135 μm in diameter) and nickel powder (100–135 μm in diameter) were hand-mixed thoroughly in an atomic ratio of Ti:Ni = 1:1 for the following tests: (i) measurement of temperature–time profile, (ii) XRD inspection of combustion-synthesized product, and (iii) combustion front quenching test. These experimental procedures were identical with those in the previous work [23]. On one hand, some of the mixture was compressed into a compact (18 mm in diameter and 20 mm in length) with a relative density of 60%. A hole was drilled at the bottom of the compact, and a thermocouple pair of W-3% Re versus W-25% Re was inserted to the center of the compact. By triggering the combustion reaction at the top of the compact after pre-heated to 573 K, the temperature–time profile was recorded as the combustion front passed through. The combustion reacted sample was then cut longitudinally and inspected by XRD (Cu Kα) to study the phase constituent. On the other hand, another compact (18 mm in diameter and 20 mm in length, relative density of 60%) was compressed in a steel die, and half of the compact was pushed out with the other half left in the die. After pre-heated to 573 K, the sample was ignited at the top surface and then quenched as the combustion front propagated into the half left in the die because the steel die absorbed heat of the reaction (see schematic illustration of the CFQM in [23]). The quenched sample with unreacted area, reacting area, and reacted area was cut longitudinally and prepared as a metallographic specimen, which was then observed by SEM, from the unreacted area to the reacted area, to trace the microstructural evolution.

Experimental results and discussion

Temperature–time profile of the combustion reaction and phase constituent of the end product

The measured temperature–time profile of the combustion reaction is shown in Fig. 1. There is one exothermic peak with a maximum temperature of 1512 K on the profile, indicating a combustion temperature (1512 K) above both the Ti-rich eutectic (about 24 at.% Ni) temperature (1215 K) and the TiNi–$TiNi_3$ eutectic (about 61 at.% Ni) temperature (1391 K) while below the melting point of TiNi (1583 K) and that of Ni (1728 K) as well as that of Ti (1943 K). In addition, the profile exhibits a nearly flat plateau region, rather than a sharp peak, and this is in good agreement with those measured by Yeh and Sung [20]. Furthermore, the XRD pattern of the combustion-synthesized product, as shown in Fig. 2, indicates that the product is composed of B2 (TiNi) and B19′(TiNi).

Microstructural evolution

Figure 3 shows an SEM photograph of the initial reactants in the unreacted zone of the quenched specimen. The EDX results showed that the gray particles were Ti and the bright ones were Ni.

Solid-state diffusion between Ti and Ni particles and locally forming of the Ti-rich melt

The change that appeared first in the reacting zone of the quenched specimen was the solid-state diffusion between Ti and Ni particles that contacted with each other, as shown

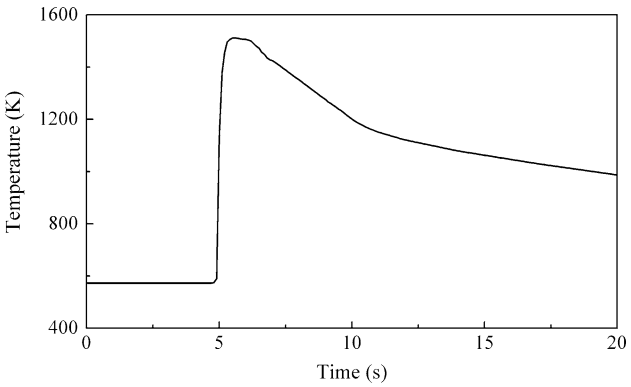

Fig. 1 Temperature–time profile during the combustion synthesis

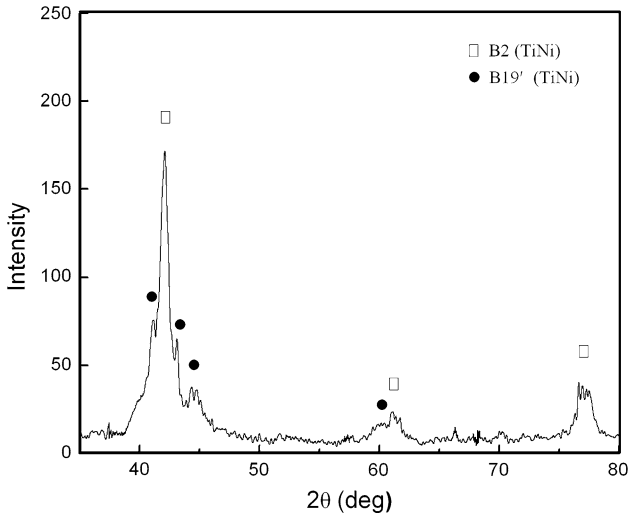

Fig. 2 XRD pattern of the combustion-synthesized product

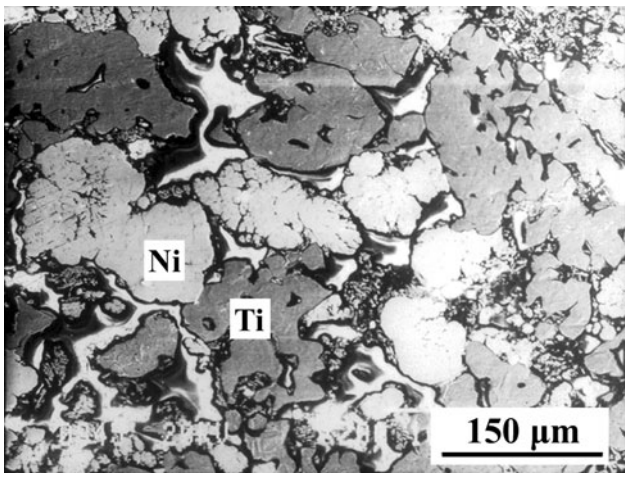

Fig. 3 SEM photograph of the initial reactants

in Fig. 4. Figure 4a shows the macrostructure of a pair of contacted Ti and Ni particles, and the microstructure of their interface is shown in Fig. 4b, from which it can be seen that two obvious reaction diffusion layers formed between the two particles. EDX results showed that the two layers were Ti_2Ni (32.21 at.% Ni) and $TiNi_3$ (70.02 at.% Ni), respectively. These results indicate that the solid-state diffusion between Ti and Ni particles that contacted with each other had occurred.

With the interdiffusion between Ti and Ni particles, the local region between Ti and Ni particles melted and resulted in the formation of Ti-rich melt, since a hyper-eutectic structure formed as it cooled in such region, as shown in Fig. 4c. EDX results showed that the block-shaped phase (28.63 at.% Ni) among the (βTi)–Ti_2Ni eutectic structure (24.17 at.% Ni) was Ti_2Ni crystallized before the eutectic as the Ti-rich melt cooled. Details of Ti-rich melt/Ni particle interface are shown in Fig. 4d, in which a TiNi reaction diffusion layer (58.17 at.% Ni) and a (Ni), Ni-matrix solid solution, diffusion layer (88.83 at.% Ni) formed one by one in the surface and subsurface of the Ni particle, respectively. Subsequently, it could be seen that in Fig. 4e, the amount of the pro-eutectic Ti_2Ni phase among the (βTi)–Ti_2Ni eutectic increased while the amount of the eutectic structure apparently decreased, indicating that the Ni particles had started to dissolve into the Ti-rich melt so that the Ni content in such melt increased. Therefore, it could be concluded that the first step of the reaction was the solid-state diffusion between Ti and Ni particles and the induced locally forming of the Ti-rich melt.

Corresponding to the equilibrium phase diagram of Ti–Ni [31], the melting point of Ti (to be exact, Ti-rich Ti–Ni alloy) decreases dramatically with increasing Ni content in the low-nickel region, so the Ti particles may melt at a temperature much lower than 1943 K, the original melting point of Ti, and even at 1215 K due to increasing Ni content. This was the case in this study and is evident in Fig. 4c, since the region where the Ti and Ni particles contacted with each other melted while other regions were still in solid state at that stage. According to this mechanism, when the temperature reached above the lowest eutectic temperature (1215 K) while Ni diffusing into the Ti particles, Ti particles melted gradually and eventually totally at a temperature much lower than the original melting point of Ti to form a Ti-rich melt, leading to dissolving of the Ni particles into such melt.

It also should be noticed that the SEM observation of the microstructural evolution in this study indicated that no TiNi formed through pre-combustion solid-state diffusion between Ti and Ni, which is in contrast to the earlier results of Biswas [11] for TE synthesis. This is because the being heated rate of the reactants in SHS mode used in this study (more than 1000 K/s, see Fig. 1) is much higher than that in TE mode (10–50 K/min, [11]), and the higher being heated rate of the reactants is not beneficial to the formation of TiNi by means of solid-state diffusion before the melting of Ti.

TiNi particles precipitating in the Ti-rich melt

With the continuous interdiffusion of Ti and Ni atoms as well as the formation of the Ti-rich melt in the manner stated above, Ti particles in the combustion front wholly melted, forming Ti-rich melt around the Ni particles, as shown in Fig. 5a. It can be seen that the TiNi particles (43.23 at.% Ni), being surrounded by Ti_2Ni (29.49 at.% Ni), precipitated in the Ti-rich melt near the Ni particle. This means that all the Ti particles melted and formed Ti-rich melt, and the Ni particles dissolved into such melt, leading to the increasing Ni content in the melt so that TiNi

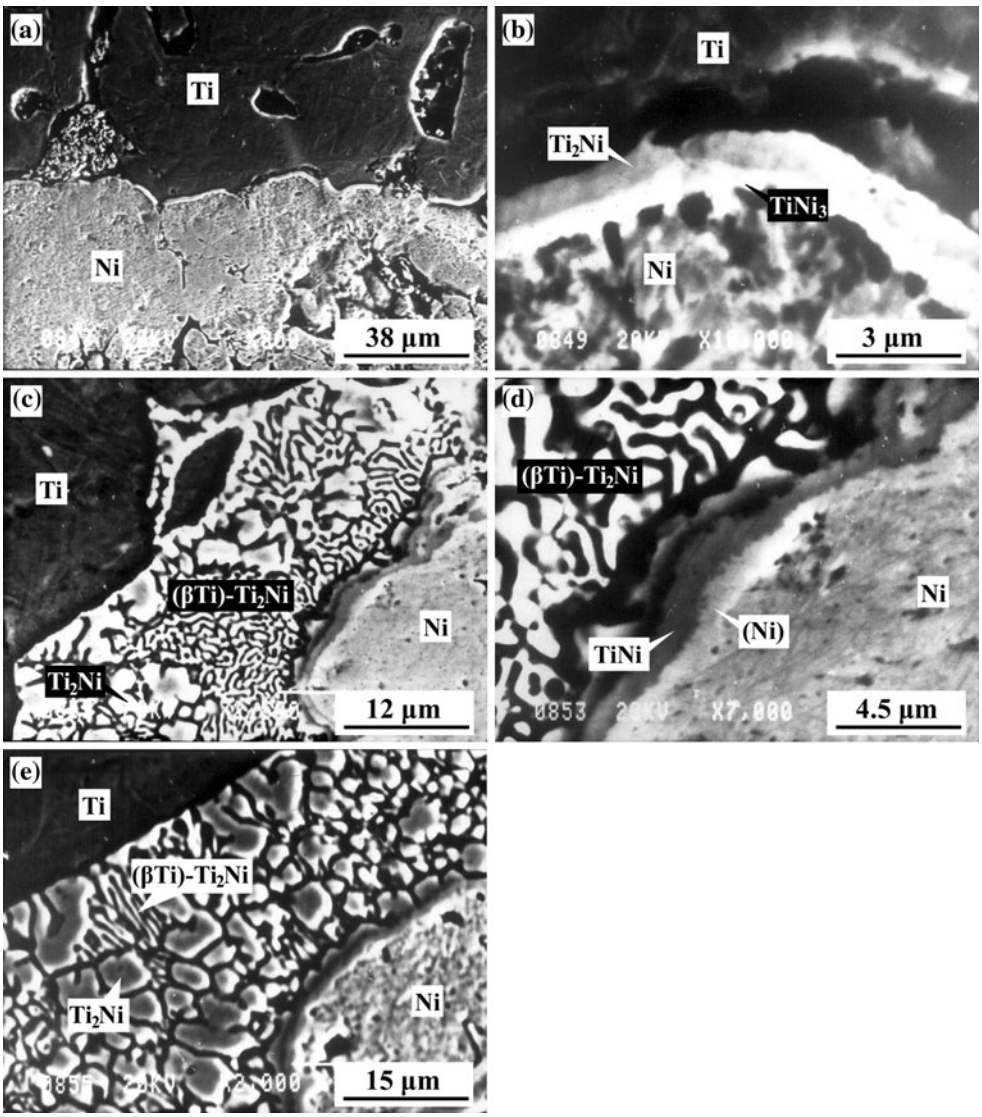

Fig. 4 SEM photographs showing: **a** reaction–diffusion layers formed in the interface region between Ti and Ni; **b** the microstructure of the interface in (**a**); **c** hypereutectic structure forming between Ti and Ni; **d** microstructure of the interface between the Ti-rich melt and Ni; **e** more Ti_2Ni precipitated in the Ti-rich melt

particles started to precipitate as the Ni content in the melt was saturated. Also, two obvious reaction diffusion layers formed one by one in the surface of the Ni particle, and EDX results showed that they were $TiNi_3$ layer (74.08 at.% Ni) and TiNi layer (45.89 at.% Ni), respectively. This is in good agreement with the equilibrium phase diagram of Ti–Ni [31] that there should be two diffusion layers, TiNi and $TiNi_3$ layers, formed between the solid-state Ni core and liquid-state Ti-rich melt, while Ti_2Ni reaction diffusion layer would be absent because of its relatively lower decomposing temperature (1257 K). With the continuously dissolving of Ni particles into the Ti-rich melt, the Ni content in the Ti-rich melt kept increasing, which is evident in Fig. 5b since the (βTi)–Ti_2Ni eutectic structure no longer exited. Subsequently, as shown in Fig. 5c, more and more TiNi particles precipitated in the saturated Ti-rich melt while the residual Ni core shrank due to the dissolving of Ni.

TiNi particles precipitating in the Ni-rich melt

It can be seen obviously in Fig. 6a that a eutectic structure formed between the TiNi layer and $TiNi_3$ layer around the Ni core as it cooled. The EDX results showed that the eutectic was the TiNi–$TiNi_3$ (58.28 at.% Ni) eutectic. This means that partial of TiNi and $TiNi_3$ layers, which contacted closely with each other around the Ni core, had melted and resulted in the formation of Ni-rich melt in this particular region. Then the Ni core and $TiNi_3$ reaction diffusion layer were exhausted, as shown in Fig. 6b, and at

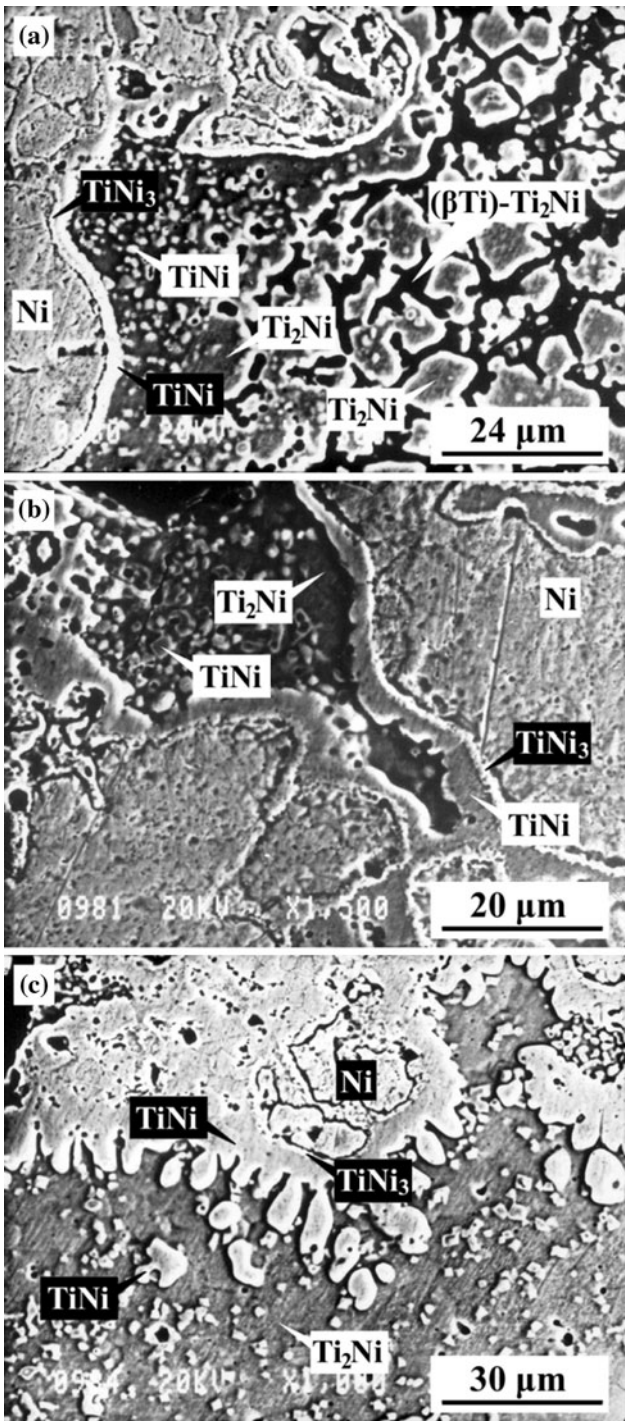

Fig. 5 SEM photographs showing: **a** TiNi particles precipitating while being coated with Ti_2Ni; **b** disappearance of the (βTi)–Ti_2Ni eutectic structure; **c** more TiNi particles precipitating in the Ti-rich melt

the same time, TiNi particles (51.93 at.% Ni) appeared among the TiNi–$TiNi_3$ eutectic structure, which is specifically shown in Fig. 6c. This indicates that the Ni core and $TiNi_3$ layer dissolved into the Ni-rich melt while simultaneously the Ti atoms outside diffused into the Ni-rich melt, thus, TiNi particles precipitated in the Ni-rich melt as the Ti content was saturated. With continuous interdiffusion of the Ti and Ni atoms, more TiNi particles precipitated in the saturated Ni-rich melt, while small amount of $TiNi_3$ phase remained in the interstices among the TiNi grains as it cooled, as shown in Fig. 6d. And it is important to notice that it should be the TiNi–$TiNi_3$ eutectic, rather than the single phase $TiNi_3$, exist in those interstices in Fig. 6d; however, there occurred the so-called divorced eutectic phenomenon so a single phase $TiNi_3$ was observed. It also should be note that the bright small particles in the TiNi particles in Fig. 6c and d were $TiNi_3$ grains crystallized as it cooled, and this is in good agreement with the phase diagram [31]. Subsequently, the residual $TiNi_3$ phase at the boundaries of TiNi grains disappeared and the isometric TiNi grains (50.65 at.% Ni) formed and occupied the previously Ni-rich region, as shown in Fig. 6e. It also can be seen in Fig. 6e that much more TiNi particles precipitated in the Ti-rich melt and much fewer $TiNi_2$ existed than those in Fig. 6b, indicating the precipitation and growing of TiNi particles, with the interdiffusion of Ti and Ni atoms, in the Ti-rich melt outside the previously Ni-rich region still continued. The needle-like phase (46.64 at.% Ni) in Fig. 6e was B19′(TiNi), which is a low temperature martensitic phase transforming from B2(TiNi) phase as it cooled rapidly. Finally, the residual Ti_2Ni phase was exhausted with sufficient interdiffusion and only B2(TiNi) phase plus B19′(TiNi) phase left in the microstructure, as shown in Fig. 6f.

The melting of partial $TiNi_3$ and TiNi reaction diffusion layers around the Ni cores is because both the Ni content in TiNi reaction diffusion layer and the Ti content in $TiNi_3$ reaction diffusion layer increased due to the interdiffusion of Ti and Ni atoms; and according to the equilibrium phase diagram of Ti–Ni [31], the melting temperature of TiNi declines with increasing Ni content in it while the amount of liquid phase increases with increasing Ti content in the $TiNi_3$ layer. Therefore, when the reaction temperature reached and exceeded the TiNi–$TiNi_3$ eutectic temperature (1391 K) with the heat released by the formation of TiNi particles in the Ti-rich melt, partial TiNi and $TiNi_3$ diffusion layers around the Ni cores would melt, forming Ni-rich melt covered by the unmelted TiNi layer. Then the residual Ni cores completely dissolved into, and the Ti atoms gradually diffused through the unmelted TiNi layer into the Ni-rich melt, so that the TiNi particles precipitated in the saturated Ni-rich melt; simultaneously, the unmelted TiNi layer would be broken up into particles because of (1) the effect of capillary action on both sides of the layer and (2) expansive force on the unmelted TiNi layer caused by the increasing of volume of the melt within the unmelted TiNi layer. After that, the Ti-rich melt and the Ni-rich melt contacted with each other, and with further interdiffusion of Ti and Ni atoms, more TiNi particles precipitated in

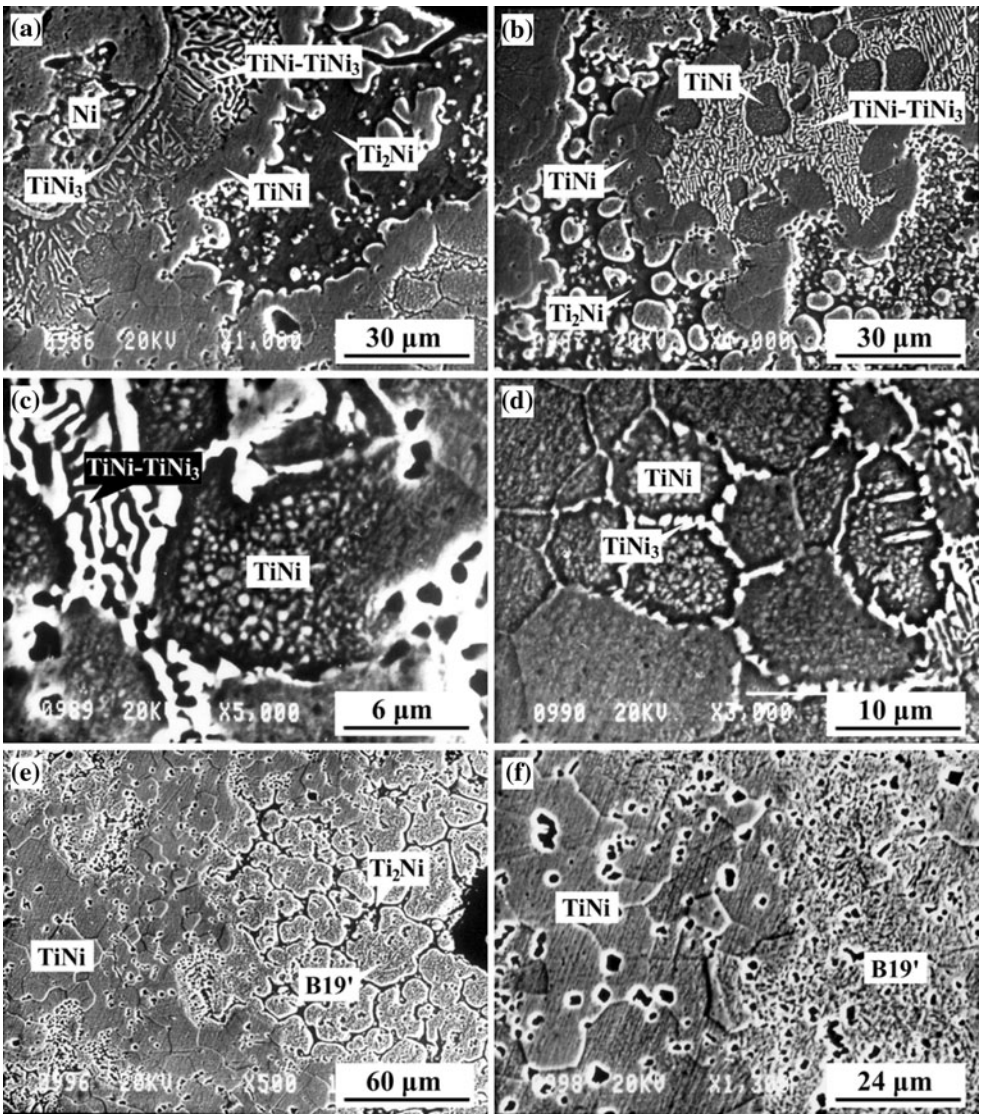

Fig. 6 SEM photographs showing: **a** TiNi–$TiNi_3$ eutectic forming between TiNi layer and $TiNi_3$ layer around the Ni particle; **b** TiNi particles appearing in the Ni-rich liquid; **c** microstructure of the TiNi particle in (**b**); **d** more TiNi precipitating in the Ni-rich liquid while less TiNi–$TiNi_3$ eutectic existing in the interstices among the TiNi grains; **e** forming of isomeric TiNi; **f** the microstructure of both the previously Ti- and Ni-rich region

Ni-rich melt, and the TiNi particles grew up in the Ti-rich melt while less and less Ti-rich melt (consequently the Ti_2Ni in the cooled microstructure) left. Combining this view and Fig. 6e, it could well explain the experimental results of Itin et al. [4] that Ti_2Ni phase in the final product was concentrated at the grain boundaries of TiNi, which was as a consequence of insufficient interdiffusion of Ti and Ni atoms at this stage.

The melting of partial TiNi and $TiNi_3$ diffusion layers should be responsible for the nearly flat plateau in Fig. 1, since the heat absorbed by the melting process and that released by the formation of TiNi were basically in balance, thus the appearance of plateau and the absence of sharp peak in the temperature–time profile are understandable. The melting of partial products during the combustion was also proved by other authors. For instance, Li et al. [15] pointed out that TiNi melted at a combustion temperature of about 1260 °C (1533 K), lower than the original melting point of TiNi (1583 K); also, Yeh and Sung [20] observed with a video camera a significant melting and shrinkage of the sample during the combustion reaction of a sample with 55% TMD and a preheating temperature of 300 °C, and the shrinkage could be attributed to, according to the analysis above, the melting of Ti particles and, more importantly, the melting of partial products.

It is interesting to notice that the melting of partial TiNi and $TiNi_3$ reaction diffusion layers is not necessary and mainly depends on the temperature can be reached during

the combustion: in the case that the reaction temperature cannot reach 1391 K, such melting would be absolutely absent, and the reaction should proceed by a dissolution–precipitation mechanism, which means only Ti particles would melt and Ni particles dissolve into the Ti-rich melt so that TiNi particles precipitate in the Ti-rich melt; while if the reaction temperature could meet the requirement for partial TiNi plus $TiNi_3$ layers to melt, the reaction should proceed by a dissolution–precipitation–diffusion mechanism, as it is in this study.

Combustion-synthesized product

Figure 7a shows a macrostructure of the combustion-synthesized product, which consists of TiNi compound and some pores. The microstructure of the TiNi compounds, as shown in Fig. 7b, is composed of B2(TiNi) and B19′(TiNi) phases. Because only TiNi particles were in solid-state after the melting of TiNi plus $TiNi_3$ diffusion layers, an as-cast product was obtained in this study. Since the melting of partial or even all of the products would introduce the shrinkage of the sample and influence the pore morphology and distribution, those want to synthesize porous TiNi by SHS should pay more attention to control the temperature during the synthesis, so the product with desired pore morphology and distribution could be obtained.

Influences of preheating

According to the microstructural evolution stated above, the combustion reaction was initiated by the melting of Ti particles at a temperature lower than the original melting point induced by the solid-state diffusion between Ti and Ni particles before the main combustion. The interdiffusion between Ti and Ni particles would indirectly lower the melting point of the Ti particles and thus accelerate the melting of Ti particles as well as the whole synthesis process, making sure that the combustion reaction will be initiated and self-sustain. Therefore, the interdiffusion between Ti and Ni particles before the main reaction is significant to the self-sustained combustion reaction. Considering that the preheating is really beneficial to the solid-state diffusion before the main combustion, preheating the compact plays an important role in the self-sustainability of the reaction. Because the interdiffusion between Ti and Ni before the main combustion is easier and faster with higher preheating temperature, and the Ti particles would, as a result, melt more quickly, so the dissolving of Ni particles is enhanced and there would be relatively more heat released since more TiNi formed in the Ti-rich melt in a relatively shorter time period. This analysis is in good agreement of that observed by Yeh and Sung [20] that the combustion temperature as well as the wave velocity increased with the increasing preheating temperature. This is also a possible explanation in the level of microstructure for the necessity of the preheating before the combustion synthesis. While in the macro-level, it can be explained as the reaction Ti + Ni → TiNi is a less-exothermic reaction [15] and the adiabatic temperature of the combustion reaction is low (reported to be 1276 °C [32]).

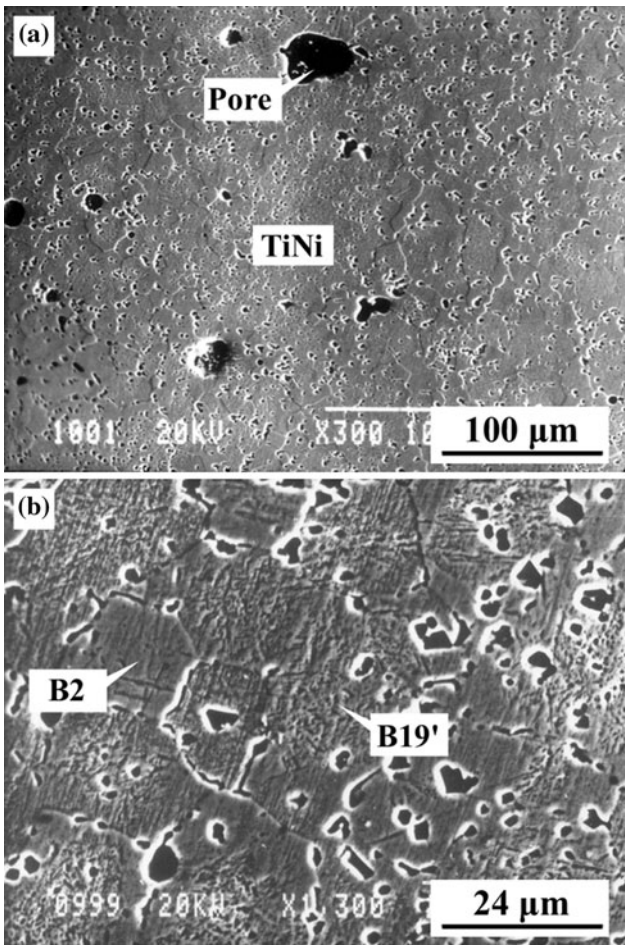

Fig. 7 SEM photographs of the combustion-synthesized product: **a** the macrostructure of the product; **b** the microstructure of the product

It seems as if the combustion front would also propagate through the compact with a solid-state mechanism in the case of preheating temperature less than 200 °C, but the reaction is not completed and the final product in those cases is the mixture of several compounds such as Ti_2Ni, $TiNi_3$ and even unreacted Ni [20]. Interestingly, the solid-state reaction mechanism, although showed significant incompleteness, may be attractive to those want to produce porous TiNi by SHS because the porous end product, rather than the relatively denser product in this study, can be obtained in that way.

Conclusions

By using an improved combustion front quenching method, a combustion front quenching test has been performed to investigate the mechanism of SHS of TiNi from Ti–Ni powder mixture under a condition of pre-heating the reactants, and the microstructural evolution in the quenched sample was analyzed with SEM and EDX. Based on the microstructural evolution in this study, it can be seen that the combustion reaction of Ti–Ni powder mixture was initiated by the solid-state diffusion between the Ti and Ni particles and proceeds by a dissolution–precipitation–diffusion mechanism, which means that the Ti particles would melt and the Ni particles would dissolve into the Ti-rich melt so that TiNi particles precipitate in the Ti-rich melt in the earlier stage of the reaction, subsequently partial TiNi plus $TiNi_3$ diffusion layers in the surface of Ni particles would melt and the formed Ni-rich melt would then contact with the Ti-rich melt, so the TiNi particles would precipitate in both Ti- and Ni-rich melts with interdiffusion of Ti and Ni atoms. Moreover, it can be deduced from the microstructural evolution that preheating temperature played an important role during the synthesis since high preheating temperature would enhance the reaction.

References

1. Otsuka K, Ren XB (1999) Intermetallics 7:511
2. Starosvetsky D, Gotman I (2001) Biomaterials 22:1853
3. Kapanen A, Ryhänen J, Danilov A, Tuukkanen J (2001) Biomaterials 22:2475
4. Itin VI, Gjunter VE, Shabalovskaya SA, Sachdeva RLC (1994) Mater Character 32:179
5. Simske SJ, Sachdeva R (1995) J Biomed Mater Res 29:527
6. Ayers RA, Simske SJ, Bateman TA, Petkus A, Sachdeva RLC, Gyunter VE (1999) J Biomed Mater Res 45:42
7. Munir ZA, Anselmi-Tamburini U (1989) Mater Sci Rep 3:277
8. Yi HC, Moore JJ (1989) J Mater Sci 24:3449. doi:10.1007/BF02385723
9. Yi HC, Moore JJ (1989) J Mater Sci 24:3456. doi:10.1007/BF02385724
10. Lee SH, Lee JH, Lee YH, Shin DH, Kim YS (2000) Mater Sci Eng A 281:275
11. Biswas A (2005) Acta Mater 53:1415
12. Kitamura K, Kuchida T, Inaba T, Tokuda M, Yoshimi Y (2006) Mater Sci Eng A 438–440:675
13. Whitney M, Corbin SF, Gorbet RB (2008) Acta Mater 56:559
14. Garay JE, Anselmi-Tamburini U, Munir ZA (2003) Acta Mater 51:4487
15. Li BY, Rong LJ, Li YY, Gjunter VE (2000) Acta Mater 48:3895
16. Dey GK (2003) Acta Mater 51:2549
17. Zhang XM, Yin WH, Wang XC (2000) Rare Met Mater Eng 29:61
18. Chung CY, Chu CL, Wang SD (2004) Mater Lett 58:1683
19. Chu CL, Chung CY, Lin PH, Wang SD (2004) Mater Sci Eng A 366:114
20. Yeh CL, Sung WY (2004) J Alloys Compd 376:79
21. Li BY, Rong LJ, Li YY, Gjunter VE (2000) Intermetallics 8:881
22. Rogachev AS, MukasYan AS, Merzhanov AG (1987) Dokl Phys Chem (English Translation) 297:1240
23. Che HQ, Fan QC (2009) J Alloys Compd 475:184
24. Fan QC, Chai HF, Jin ZH (2001) J Mater Sci 36:5559. doi:10.1023/A:1012597111988
25. Fan QC, Chai HF, Jin ZH (2002) J Mater Sci 37:2251. doi:10.1023/A:1015313215455
26. Fan QC, Chai HF, Jin ZH (2002) Intermetallics 10:541
27. Xiao GQ, Fan QC, Gu MZ, Jin ZH (2006) Mater Sci Eng A 425:318
28. Xiao GQ, Fan QC, Gu MZ, Jin ZH (2007) J Wuhan Univ Technol Mater Sci Ed 22:502
29. Xiao GQ, Fan QC, Gu MZ, Wang ZH, Jin ZH (2004) Mater Sci Eng A 382:132
30. Li Y, Nan YX, Guo WX, Che HQ, Fan QC (2010) Intermetallics 18:179
31. Baker H (1992) ASM Handbook, vol 3: alloy phase diagrams. ASM International, Materials Park
32. Bratchikov AD, Merzhanov AG, Itin VI, Khachin VM, Dudarev EF, Gyunter VE, Maslov VM, Chernov DB (1980) Sov Powder Metall Met Ceram 19:5